White Rose Research Online

eprints@whiterose.ac.uk
https://eprints.whiterose.ac.uk
Universities of Leeds, Sheffield and York

Deposited via The University of Sheffield.

White Rose Research Online URL for this paper:
https://eprints.whiterose.ac.uk/id/eprint/89079/

Version: Accepted Version

Article:
Yang, W-G., Morley, N.A., Sharp, J. et al. (2015) Giant electric field tunable magnetic properties in a Co50Fe50/lead magnesium niobate-lead titanate multiferroic heterostructure. Journal of Physics D: Applied Physics, 48 (30). ISSN: 0022-3727

https://doi.org/10.1088/0022-3727/48/30/305005

Reuse
Items deposited in White Rose Research Online are protected by copyright, with all rights reserved unless indicated otherwise. They may be downloaded and/or printed for private study, or other acts as permitted by national copyright laws. The publisher or other rights holders may allow further reproduction and re-use of the full text version. This is indicated by the licence information on the White Rose Research Online record for the item.

Takedown
If you consider content in White Rose Research Online to be in breach of UK law, please notify us by emailing eprints@whiterose.ac.uk including the URL of the record and the reason for the withdrawal request.

IOP Publishing Journal of Physics D: Applied Physics
J. Phys. D: Appl. Phys. **00** (2015) 000000 (7pp) UNCORRECTED PROOF

Giant electric field tunable magnetic properties in a $Co_{50}Fe_{50}$/lead magnesium niobate–lead titanate multiferroic heterostructure

Wei-Gang Yang, Nicola A Morley, Joanne Sharp and W Mark Rainforth

Department of Materials Science and Engineering, University of Sheffield, Sheffield, UK

E-mail: m.rainforth@sheffield.ac.uk

Received 10 March 2015, revised 13 May 2015
Accepted for publication 9 June 2015
Published

Abstract

$Co_{50}Fe_{50}$/(0 1 1)-oriented lead magnesium niobate–lead titanate (PMN–PT) multiferroic (MF) heterostructures were fabricated by RF sputtering magnetic films onto PMN–PT substrates. The effect of magnetic layer thickness (30 nm to 100 nm) on the magnetoelectric (ME) coupling in the heterostructures was studied independently, due to the almost constant magnetostriction constant ($\lambda = 40 \pm 5$ ppm) and similar as-grown magnetic anisotropies for all studied magnetic layer thicknesses. A record high remanence ratio (M_r/M_s) tunability of 95% has been demonstrated in the 65 nm $Co_{50}Fe_{50}$/PMN–PT heterostructure, corresponding to a large ME constant (α) of 2.5×10^{-6} s m^{-1}, when an external electric field (E-field) of 9 kV cm^{-1} was applied. Such an MF heterostructure provides considerable opportunities for E-field-controlled multifunctional devices.

Keywords: multiferroic heterostructure, magnetoelectric coupling, cobalt iron film (CoFe), microstructure

AQ1 (Some figures may appear in colour only in the online journal)

1. Introduction

Recently, the use of an electric field (E-field) to control the magnetic properties in multiferroic (MF) materials (converse magnetoelectric effect, CME [1]) rather than a magnetic field generated by a current [2] or the current itself [3] has drawn intensive interest due to the important potential applications of these materials such as magnetoelectric random access memory (MERAM) devices [4–7] and magnetoelectric sensors [8, 9]. Single phase MF materials are rare in nature [10] and almost all of them show only a weak magnetoelectric (ME) coupling below room temperature [1]. Therefore, most research has focused on MF composites. Many papers have reported the strain-induced magnetization changes in a wide range of MF layered composites (ferromagnetic (FM) films/ferroelectric (FE) substrates) such as Fe-Ga/(1 1 0) PMN–PT [11], $Ni_{80}Co_{20}$/(1 1 0) PZN–PT (lead zinc niobate–lead titanate) [12], FeGaB(1 1 0) PZN–PT [13], Fe_3O_4/PZN–PT [14], $NiFe_2O_4$/(0 0 1) PMN–PT [15] and Ni/(1 1 0) PMN–PT [16].

Kim *et al* [17] studied the effects of the thickness and composition of the magnetic Co_xPd_{1-x} layer on the ME coupling strength. The ME constant (α) increased from 2×10^{-7} s m^{-1} to 2.5×10^{-7} s m^{-1} as the film thickness of $Co_{0.25}Pd_{0.75}$ decreased from 30 nm to 10 nm. However, for both $Co_{0.22}Pd_{0.0.78}$ and $Co_{0.18}Pd_{0.0.82}$ compositions, α for the 10 nm thick magnetic film was lower than that for the 20 nm thick magnetic film due to the change of perpendicular magnetic anisotropy (PMA) at 10 nm. In addition, for ultrathin magnetic layers (<20 nm), the magnetostriction constant (λ) can be strongly influenced by the thickness [18] according to the formula $\lambda = \lambda_b + \lambda_i/t$, where λ_b is the magnetostriction of the bulk, λ_i is the interfacial contribution and t is the magnetic layer thickness [19]. However, the effect of varying λ with t on ME coupling was not considered by Kim *et al*.

 © 2015 IOP Publishing Ltd Printed in the UK

JNL:JPD PIPS: 516038 TYPE: PAP TS: NEWGEN DATE:26/6/15 EDITOR: IOP SPELLING: US

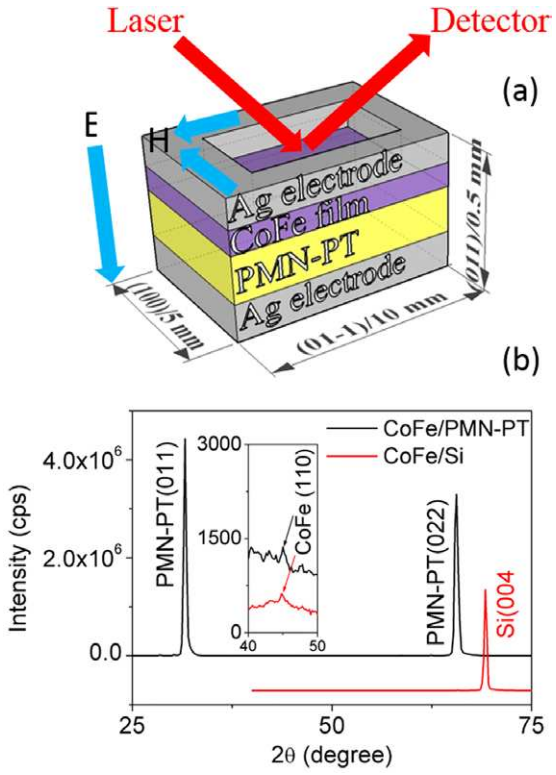

Figure 1. (a) A schematic diagram of a CoFe/500 μm (0 1 1) PMN–PT heterostructure. Magnetic properties were measured by the MOKE system. (b) XRD spectra of CoFe/PMN–PT and CoFe/Si heterostructures.

In this study, $Co_{50}Fe_{50}$ (CoFe) film was chosen to be the FM layer due to excellent soft magnetic properties, relatively high magnetostriction [20, 21] and large saturated magnetization [22]. The (0 1 1)-oriented PMN–PT [23] was considered as the FE substrate due to its large in-plane anisotropic strains. The effect of magnetic layer thickness on ME coupling in CoFe/PMN–PT heterostructures was investigated over a much wider thickness range, from 30 nm to 100 nm. The in-plane magnetic anisotropies of all as-grown samples were similar, which ruled out the influence of magnetic anisotropy on ME coupling. A record high remanence ratio (M_r/M_s) tunability of 95% was demonstrated in the 65 nm CoFe/PMN–PT heterostructure, corresponding to a ten times larger α of 2.5×10^{-6} s m^{-1} than in the CoPd/(0 0 1) PMN–PT system [17]. The reason is a large transverse anisotropic strain [24] produced in (0 1 1) PMN–PT by the *E*-field, which significantly contributes to the change of in-plane magnetic anisotropy of the magnetic layer [11].

2. Experiments

We deposited 30 nm, 45 nm, 65 nm and 100 nm thick CoFe films on the (0 1 1) PMN–PT substrate at room temperature by RF sputtering in a Nordiko NM2000 RF deposition system. To achieve a smooth surface, the substrate was cold-mounted into epoxy resin mixed with epoxy hardener after being wrapped with PMMA. The cold-mounted substrate was then polished on Automet grind and polish equipment using a series of polish suspensions. The PMMA was dissolved by acetone and then the sample was taken out from the hardened resin. The polished substrate was cleaned prior to use with acetone and IPA. The sputtering power, working pressure and base pressure were 75 W, 5.0 $\pm$ 0.1 mTorr and 1.2 $\pm$ 0.2 $\times$ 10^{-3} mTorr, respectively. An *in situ* magnetic field was applied along the (1 0 0) or (0 1-1) crystallographic direction of the PMN–PT substrate during the growth of the CoFe film. The (0 1 1)-oriented PMN–PT (10 cm (0 1 $-$ 1) $\times$ 5 cm (1 0 0) $\times$ 0.5 cm (0 1 1)) had anisotropic strains with in-plane piezoelectric coefficients of $d_{31} = -1500$ to -2000 pC/N and $d_{32} = 500$–700 pC N^{-1} reported by the supplier. The PMN–PT was prepoled through the thickness at an *E*-field of 5 kV cm^{-1} for 10 min before being used as a substrate. Conductive silver paint was used as the electrodes on the top CoFe surface and the bottom PMN–PT surface for the applied *E*-field. Magneto-optical Kerr effect (MOKE) measurements were used to investigate the magnetic properties when a series of dc *E*-fields were applied to MF heterostructures. The transverse geometry MOKE system was used, which is sensitive to the in-plane component of magnetization perpendicular to the plane of laser incidence. A solid state laser diode of wavelength about 635 nm was used. The skin depth of the laser is about 10–20 nm at this wavelength for metallic films. A space was left on the CoFe surface for the reflection of the laser. The polarizer angle was set at 142° so that the laser is plane polarized before falling onto the film. After reflecting from the film, the laser beam passed through an analyser and was then detected by a photodetector. A well polished substrate surface was required to avoid the obvious laser scattering and thus enhance the ratio of signal to noise. The magnetic field was applied along the (1 0 0) or (0 1 $-$ 1) direction of the PMN–PT, while the *E*-field was applied along the (0 1 1) direction of the PMN–PT, as shown in figure 1(a). The positive *E*-field was referred to be parallel to the prepolarization of the substrate, while the negative *E*-field was referred to be antiparallel. The effective saturation magnetostriction constants (λ) were measured using a technique [25, 26] based on the Villari effect. Because it is difficult to directly measure λ of the CoFe film on the PMN–PT substrate, it was estimated by measuring the same grown CoFe film on a Si substrate. The sample was strained by bending tools with different known radii *R*, i.e. 300 mm, 400 mm and 500 mm. MOKE measurements were made at each band radius. For each loop, the effective saturation fields H_{eff} were taken at $M_r/M_s = 0.96$, 0.97 and 0.98. These H_{eff} values were plotted as a function of the inverse band radii ($1/R$) and then the gradient of each line was determined. Finally, the λ was determined from [25, 26]

$$\lambda = \frac{\mathrm{d}H_{\text{eff}}}{\mathrm{d}(1/R)} \frac{2\mu_0 M_s(1-\nu_s^2)}{3t_s Y_s} \tag{1}$$

where the saturation induction $\mu_0 M_s$ was 2.4 T [22]. The Poisson ratio ν_s and Young's modulus Y_s for the (1 0 0) Si substrate were 0.28 and 130 GPa [27, 28]. The Si substrate thickness t_s was 380 $\pm$ 50 μm.

To investigate the microstructure of the heterostructure, x-ray diffraction (XRD) measurements were made on the sample without the top Ag electrode using a Siemens D5000 x-ray diffractometer with Cu K_α radiation (λ = 1.540 56 Å).

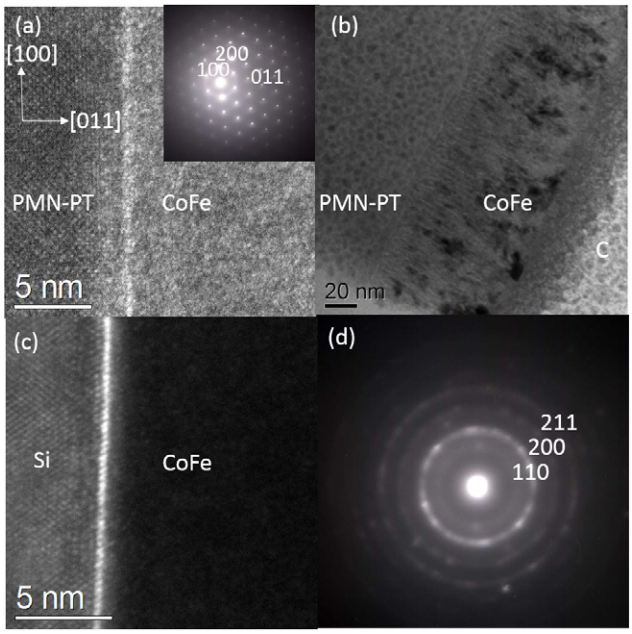

Figure 2. (a), (b) Cross-sectional HRTEM image (a) and TEM image (b) of the CoFe/PMN–PT heterostructure. (c) Cross-sectional HRTEM image of CoFe/Si heterostucture. (c) inset, (d) SAED patterns of PMN–PT and CoFe film, respectively.

The x-ray beam before and after incidence on the specimen was collimated with both the divergence slit and the anti-scattering slit 0.6° wide. The x-ray diffractometer was run at a scan speed of 0.5 deg min^{-1}. Cross-sectional transmission electron microscopy (TEM) specimens were prepared by focused ion beam (FIB) in an FEI Quanta 200 3D. A specimen foil about 2 μm thick was *in situ* lifted out by an Omniprobe and then it was attached to a TEM grid. Next, it was gradually thinned by varying the current ion beam from 0.5 nA to 30 pA. Finally, the fabricated TEM specimens were observed on both an FEI Tecnai T20 and a JEOL 2010F operating at 200 kV.

3. Results and discussion

Figure 1(b) shows a XRD result for CoFe/PMN–PT and CoFe/Si heterostructures. It shows strong (0 1 1) and (0 0 4) diffraction peaks of PMN–PT and Si substrates, respectively. The weak (1 1 0) diffraction peak of the CoFe film is seen only on a much smaller scale of intensity, as shown in the inset. This indicates that the films are not grown epitaxially on both substrates as expected.

To understand the microstructure of the magnetic film and interface in the heterostructure in more detail, cross-sectional high-resolution transmission electron microscopy (HRTEM) images are shown in figures 2(a) and (c). The heterostructure shows a well defined interface between the CoFe film and PMN–PT substrate. Figure 2(b) shows a uniform columnar growth structure of the CoFe film and an average columnar grain size of 3.3 ± 0.5 nm, which is comparable with that of ~5 nm in the Fe-Ga/PMN–PT system [11]. The selected area electron diffraction (SAED) pattern in figure 2(d) shows the polycrystalline structure of the CoFe film, and that the columnar grains are composed of randomly oriented nanocrystals. The crystalline plane of (1 1 0) in the CoFe film shows the strongest diffraction, which is well consistent with the XRD results for the CoFe film.

Figures 3(a)–(d) show the electrical dependence on the magnetic hysteresis loops of CoFe/(0 1 1) PMN–PT heterostructures for the series of CoFe thicknesses. In figures 3(a)–(c), the hysteresis loops were measured along the (1 0 0) direction of PMN–PT, while in figure 3(d), the hysteresis loops were measured along (0 1 − 1) due to stronger coupling along this direction than (1 0 0). The insets show similar in-plane magnetic anisotropy for all the samples' thicknesses. In these samples, both the magnetic properties and anisotropy were changed greatly by the applied *E*-fields. In particular, it is noted that a significant anisotropy change was observed in the 65 nm thick sample. An initial in-plane magnetic anisotropy was induced by the *in situ* magnetic field. When the *E*-field-induced strains were applied on the magnetic film, the strain-induced anisotropy change could be described as [17]

$$\Delta K = \frac{-3\lambda\varepsilon Y}{2(1-v)} \tag{2}$$

where v and Y are the Poisson's ratio and Young's modulus of the FM film. λ is the magnetostriction constant, about 40 ± 5 ppm. The compressive strain ε created along (1 0 0) is estimated to be 2000 ppm [29]. Therefore, the *E*-field-induced anisotropy energy is positive along (1 0 0) and thus anisotropy energy increases when applying the *E*-field, which consequently deters magnetization alignment along the (1 0 0) direction, i.e. the magnetic hard axis, and vice versa the tensile strain ε created along (0 1 − 1) induces negative anisotropy energy, which favors magnetization alignment along the (0 1 − 1) direction, i.e. the magnetic easy axis. The change of magnetic remanence ratio (M_r/M_s) induced by the *E*-field of 9 kV cm^{-1} is greatly enhanced from 46% to 95% by reducing the thickness of the CoFe layer from 100 nm to 65 nm, as shown in figure 3(f). However, when the CoFe layer thickness is further reduced to 45 nm and 30 nm, the maximum changes of M_r/M_s are induced at the *E*-fields of 3 kV cm^{-1} and 2 kV cm^{-1}, respectively. For both thinner CoFe layers, when the *E*-fields increase further, the coercive fields (H_c) are increased significantly. As shown in figure 3(e), the changes of H_c (ΔH_c) are up to 11.5 kA m^{-1} (144 Oe) and11 kA m^{-1} (138 Oe) at the *E*-fields of 5 kV cm^{-1} and 3 kV cm^{-1} for CoFe layers 45 nm thick and 30 nm thick, respectively. Also, H_c increases as the *E*-field continues to increase. ΔH_c achieves a maximum of 17.5 kA m^{-1} (220 Oe) at the *E*-field of 7 kV cm^{-1} in the 45 nm thick sample, which is five times larger than the H_c of 3.5 kA m^{-1} (44 Oe) without *E*-field. The value of ΔH_c is also much larger than the 3.5 Oe and 22.93 Oe reported previously in the CoFe/PZT system [30] and CoFeB/SiO_2/PMN–PT system [31], respectively.

The ME coupling constant α can be defined as $\alpha = \mu_0 \Delta M_r/E$, where μ_0 is the permeability of free space [32]. The value of ΔM_r is estimated from the experimental result of *E*-field induced M_r/M_s change ($\Delta M_r/M_s$) and saturated magnetization M_s (~1900 emu cm^{-3}) taken from [22, 33]. For example, for

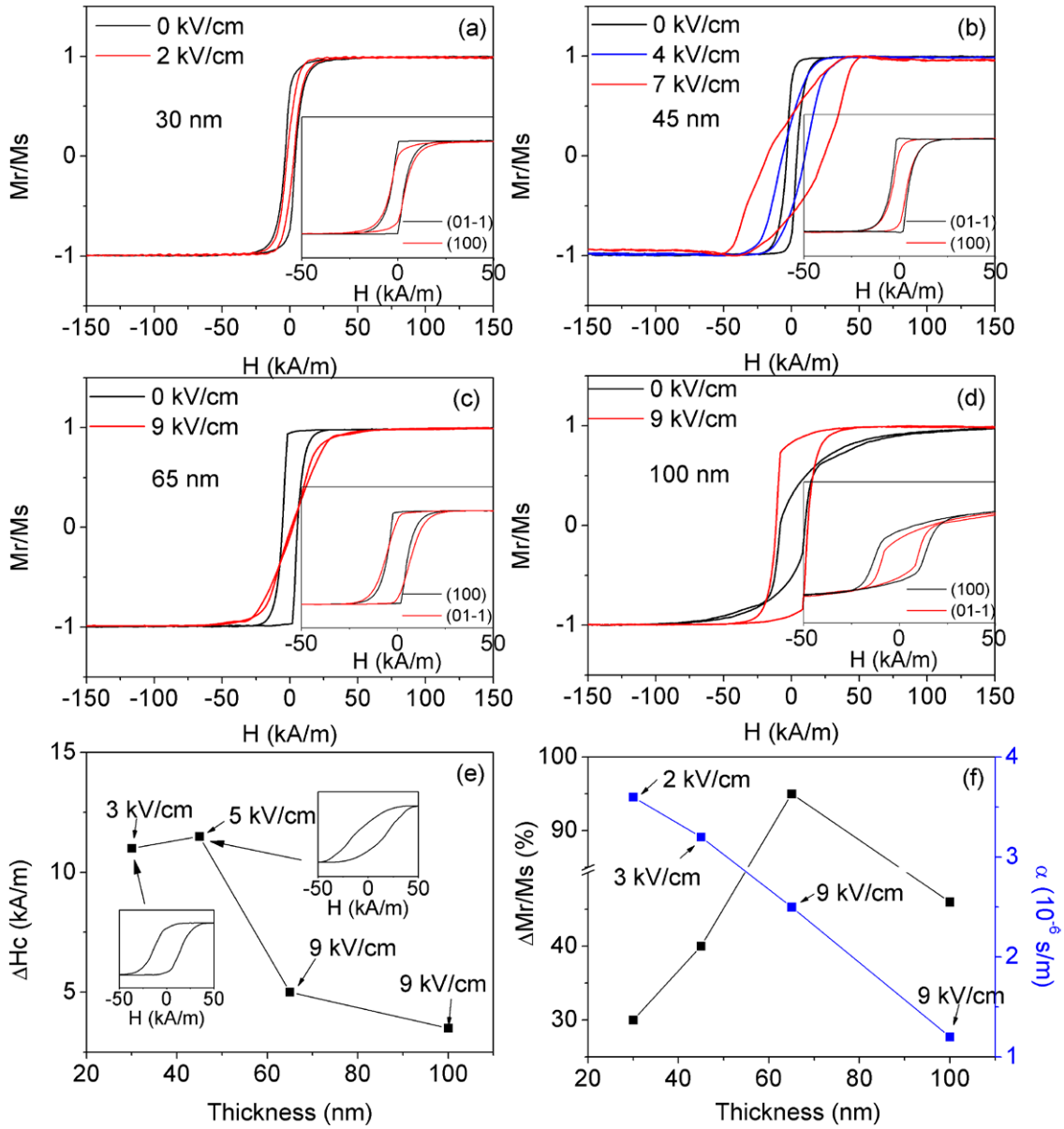

Figure 3. (a)–(d) Electric dependence of magnetic hysteresis loops in CoFe/(0 1 1)PMN–PT heterostructure on thickness of CoFe layer. The insets show easy and hard axis loops of as-grown samples without the *E*-field. (e) Absolute values of coercive field (H_c) changes with CoFe thickness (f) Absolute values of remanence ratios (M_r/M_s) and ME constant (α) changes with CoFe thickness.

a CoFe layer thickness of 65 nm, the ME coupling constant $\alpha = \mu_0 \Delta M_r/E = 4\pi \times 10^{-7} \times (1900\,\text{emu cm}^{-3}) \times 0.95/(9\,\text{kV cm}^{-1})$ $= 2.5 \times 10^{-6}\,\text{s m}^{-1}$. To understand the effect of magnetic layer thickness on α, it is described as [17]

$$\begin{aligned}\alpha &= \mu_0 \Delta M_r/E = (\varepsilon_{FM}/\varepsilon_{FE}) \times (\mu_0 \Delta M_r/\varepsilon_{FM}) \times (\varepsilon_{FE}/E) \\ &= n \times (\varepsilon_{FM}/\varepsilon_{FE}) \times \lambda\lambda \times d_{ij}\end{aligned} \quad (3)$$

where ε_{FM} and ε_{FE} represent strains of the FM and FE layers, respectively. d_{ij} is the in-plane piezoelectric constant of the FE layer and n is a constant. The experimental magnetostriction constant λ remains almost constant at about 40 ± 5 ppm for these bulk-like films (>20 nm), such that λ is 29 ± 7 ppm, 35 ± 3 ppm and 40 ± 3 ppm for the thickness 30 nm, 35 nm and 65 nm respectively, which is almost consistent with the λ of 47 ± 4 ppm reported for a 50 nm CoFe film [21]. The trends show that the value of λ gradually approaches that of bulk, as shown in the formula $\lambda = \lambda_b + \lambda_i/t$ above, due to the reduction in the interfacial contribution with increasing film thickness [19]. The last term of equation (3), d_{ij}, is also constant due to the same PMN–PT substrates being used. Therefore, α is eventually determined by the term $\varepsilon_{FM}/\varepsilon_{FE}$, which increases as FM layer thickness reduces due to the reduced relaxation of ε_{FM} in the thin FM layer. In figure 3(f), α increases from $1.2 \times 10^{-6}\,\text{s m}^{-1}$ to $2.5 \times 10^{-6}\,\text{s m}^{-1}$ at 9 kV cm^{-1} when CoFe thickness reduces from 100 nm to 65 nm, which is consistent with equation (3). When CoFe thickness continues to reduce to 45 nm and 30 nm, α increases only at a lower *E*-field strength of 3 kV cm^{-1} and 2 kV cm^{-1}, respectively. The reason for this is that the giant ε_{FM} in the thinner CoFe layers created by the FE layer results in domain wall pinning [34], which causes a significant increase in H_c.

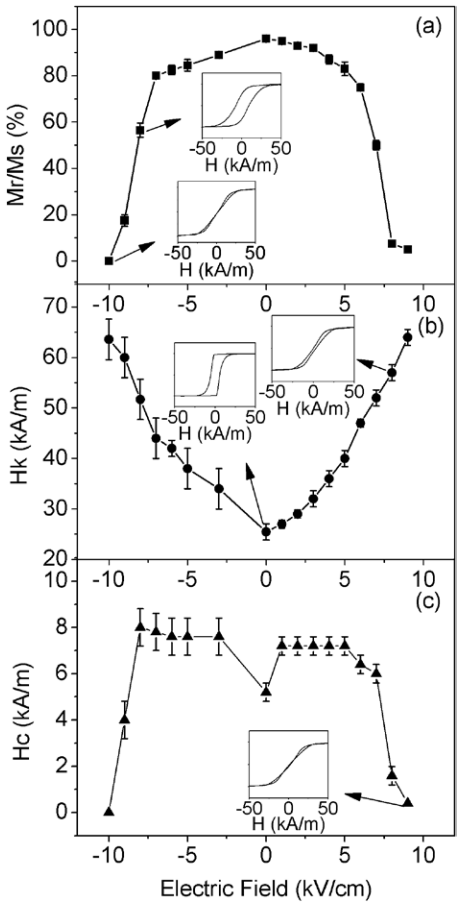

Figure 4. The normalized remanent magnetization (M_r/M_s) (a), saturation field (H_k) (b) and coercive field (H_c) (c) measured along the (1 0 0) direction as a function of applied E-field in the 65 nm CoFe/PMN–PT heterostructure.

In this study, α is two orders of magnitude larger than the 6×10^{-8} s m^{-1} in the epitaxial $La_{0.67}Sr_{0.33}$ MO_3/(0 0 1) PMN–PT system [35]. However, some large ME coupling constants α of 8×10^{-7} s m^{-1} and 4.55×10^{-7} s m^{-1} were recently reported in a CoPd/PMN–PT system [17] and Fe-Ga/PMN–PT system [11], respectively. The giant coupling constant is attributed to the combination of a few crucial properties: a small film thickness (⩽100 nm), large magnetostriction constant, saturation magnetization and M_r/M_s in our sputtered $Co_{50}Fe_{50}$ film and the high in-plane piezoelectric coefficient PMN–PT substrate with smooth surface, which provides an effective elastic coupling at the interface between the CoFe film and the PMN–PT substrate.

Figure 4 shows the detailed variation in M_r/M_s, H_k and H_c taken from the magnetic hysteresis loops measured along the (1 0 0) direction of the PMN–PT at each applied E-field in the 65 nm CoFe/PMN–PT heterostructure. Both positive and negative E-fields were applied through the substrate thickness. The changes in the magnetic properties and magnetic anisotropy induced by the positive and negative E-fields were similar, which indicates an almost symmetric piezoelectric strain variation against the E-field. With increasing E-field strength from 0 kV cm^{-1} to 9 kV cm^{-1}, M_r/M_s is reduced from 95.5% to 0.5%, while the saturation field (H_k) is increased from

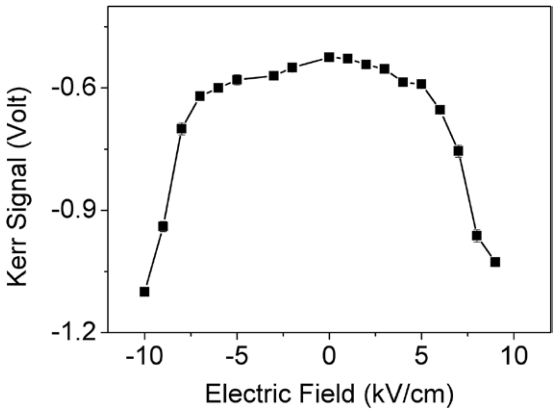

Figure 5. The Kerr signal variation as a function of the applied E-field at magnetic field $H = 0$ kA m^{-1}.

25.5 kA m^{-1} to 63.7 kA m^{-1}. The compressive strain is created along (1 0 0) because of the negative piezoelectric coefficient ($d_{31} = -1500$ to -2000 pC N^{-1}), which causes the increase in H_k due to the positive magnetostriction constant of CoFe. The increased H_k forces the in-plane magnetization to rotate from the direction of (1 0 0) to (0 1 $-$ 1) and thus leads the reduction of M_r/M_s along (1 0 0). Interestingly, H_k changed almost linearly with E-field, while M_r/M_s and H_c changed significantly from 6 kV cm^{-1} to 8 kV cm^{-1}, which was attributed to a high transverse strain from the orthorhombic to rhombohedral (R) phase transition induced by the E-field [24]. To further investigate the converse ME coupling effect, the E-field-controlled magnetization change is shown in figure 5 at magnetic field $H = 0$ kA m^{-1}. In the MOKE system, the Kerr signal measured is linearly proportional to the Kerr effect and thus the magnetization of the film. Therefore, the Kerr signal is used to represent the magnitude of magnetization in the film. A significant change in Kerr signal is observed with variation of the E-field, which provides great opportunities for E-field-independent controlled magnetization. The Kerr signal change is up to 96% from -0.525 ± 0.003 V to -1.027 ± 0.01 V when the E-field of 9 kV cm^{-1} is applied, which is consistent with the change of 95% taken from M_r measurement.

For such strong strain-mediated magnetization, the origin from the large magnetostriction effect is widely reported now for a thick monolayer metal film on a FE substrate (PMN–PT). However, there may be another potential contribution from the strain effect on interfacial coupling [36] in a system based on orbital hybridization. In the CoFe/PMN–PT heterostructure, a large lattice mismatch (~28.9%) exists due to the distinct in-plane lattice parameters of $a_{CoFe} = 2.858$ Å [37] and $a_{PMN-PT} = 4.021$ Å [36]. The polycrystalline CoFe films grown on PMN–PT are likely to be under weak tensile strain. When the compressive strain induced by the E-field is applied it will partly release the tensile strain, which may result in stronger orbital hybridization between the atoms and thus stronger interfacial coupling [36]. For example, d orbital hybridization between Ti and Fe reported in the Fe/$BaTiO_3$ system [38] was enhanced when the E-field was applied. This was due to the displacements of atoms at the interface created by FE instability, which changed the overlap between atomic orbitals at

the interface and thus changed the interfacial magnetization [38]. However, in most cases, the strain effects on the interfacial coupling mechanism are used to explain an epitaxial ultrathin magnetic film system (<5 nm) because the interfacial contribution to the magnetization is known to be very weak in bulk-like films. More work on the strain effect on the interfacial coupling mechanism in polycrystalline thick film systems remains to be done.

4. Conclusion

In conclusion, we have demonstrated a record high remanence ratio (M_r/M_s) tunability of 95%, with a corresponding giant ME constant α of 2.5 $\times$ 10^{-6} s m^{-1} in a CoFe/PMN–PT multiferroic composite at a maximum applied E-field of 9 kV cm^{-1}. The ME constant α has been obviously improved by reducing the magnetic layer thickness in MF heterostructures. Such MF composites provide great opportunities for E-field-controlled multifunctional devices.

Acknowledgment

This work is financially supported by a University of Sheffield Prize Scholarship.

AQ2 ## References

[1] Ma J, Hu J M, Li Z and Nan C W 2011 Recent progress in multiferroic magnetoelectric composites: from bulk to thin films *Adv. Mater.* **23** 1062–87
[2] Prinz G A 1998 Device physics—magnetoelectronics *Science* **282** 1660–3
[3] Myers E B, Ralph D C, Katine J A, Louie R N and Buhrman R A 1999 Current-induced switching of domains in magnetic multilayer devices *Science* **285** 867–70
[4] Chen X, Hochstrat A, Borisov P and Kleemann W 2006 Magnetoelectric exchange bias systems in spintronics *Appl. Phys. Lett.* **89** 202508
[5] Hu J M, Li Z, Chen L Q and Nan C W 2011 High-density magnetoresistive random access memory operating at ultralow voltage at room temperature *Nat. Commun.* **2** 553
[6] Bibes M and Barthélémy A 2008 Multiferroics: towards a magnetoelectric memory *Nat. Mater.* **7** 425–6
[7] Hu J M, Li Z, Chen L Q and Nan C W 2012 Design of a voltage-controlled magnetic random access memory based on anisotropic magnetoresistance in a single magnetic layer *Adv. Mater.* **24** 2869–73
[8] Zhai J Y, Xing Z P, Dong S X, Li J F and Viehland D 2006 Detection of pico-Tesla magnetic fields using magnetoelectric sensors at room temperature *Appl. Phys. Lett.* **88** 062510
[9] Israel C, Mathur N D and Scott J F 2008 A one-cent room-temperature magnetoelectric sensor *Nat. Mater.* **7** 93–4
[10] Hill N A 2000 Why are there so few magnetic ferroelectrics? *J. Phys. Chem.* B **104** 6694–709
[11] Zhang Y, Wang Z G, Wang Y J, Luo C T, Li J F and Viehland D 2014 Electric-field induced strain modulation of magnetization in Fe-Ga/Pb($Mg_{1/3}Nb_{2/3}$)-$PbTiO_3$ magnetoelectric heterostructures *J. Appl. Phys.* **115** 084101
[12] Liu M, Li S D, Obi O, Lou J, Rand S and Sun N X 2011 Electric field modulation of magnetoresistance in multiferroic heterostructures for ultralow power electronics *Appl. Phys. Lett.* **98** 222509
[13] Liu M, Zhou Z Y, Nan T X, Howe B M, Brown G J and Sun N X 2013 Voltage tuning of ferromagnetic resonance with bistable magnetization switching in energy-efficient magnetoelectric composites. *Adv. Mater.* **25** 1435–9
[14] Liu M *et al* 2009 Giant electric field tuning of magnetic properties in multiferroic ferrite/ferroelectric heterostructures *Adv. Funct. Mater.* **19** 1826–31
[15] Park J H, Jeong Y K, Ryu S, Son J Y and Jang H M 2010 Electric-field-control of magnetic remanence of $NiFe_2O_4$ thin film epitaxially grown on Pb($Mg_{1/3}Nb_{2/3}$)O_3–$PbTiO_3$ *Appl. Phys. Lett.* **96** 192504
[16] Wu T, Bur A, Zhao P, Mohanchandra K P, Wong K, Wang K L, Lynch C S and Carman G P 2011 Giant electric-field-induced reversible and permanent magnetization reorientation on magnetoelectric Ni/(0 1 1)[Pb($Mg_{1/3}Nb_{2/3}$)O_3](1−x)–[$PbTiO_3$]$_x$ heterostructure *Appl. Phys. Lett.* **98** 012504
[17] Kim J H, Ryu K S, Jeong J W and Shin S C 2010 Large converse magnetoelectric coupling effect at room temperature in CoPd/PMN–PT (0 0 1) heterostructure *Appl. Phys. Lett.* **97** 252508
[18] Ounadjela K, Lefakis H, Speriousu V S, Hwang C and Alexopoulos P S 1989 Effect of surface composition observed by Auger electron spectroscopy on magnetization and magnetostriction of NiFe and NiFeRh thin films *J. Appl. Phys.* **65** 1230–3
[19] Fukuzawa H, Kamiguchi Y, Koi K, Iwasaki H and Sahashi M 2002 Saturation magnetostriction of an ultrathin CoFe free-layer on double-layered underlayers *J. Appl. Phys.* **91** 3120–4
[20] Hall R C 1960 Magnetic anisotropy and magnetostriction of ordered and disordered cobalt–iron alloys *J. Appl. Phys.* **31** S157–8
[21] Jung H S, Doyle W D, Wittig J E, Al-Sharab J F and Bentley J 2002 Soft anisotropic high magnetization Cu/FeCo films *Appl. Phys. Lett.* **81** 2415–7
[22] Rengarajan S, Yun E J, Kang W S and Walser R M 1997 Effect of intermixing on the magnetic properties of $Co_{50}Fe_{50}$/$Ni_{80}Fe_{20}$ multilayers *J. Appl. Phys.* **81** 4761–3
[23] Baek S H *et al* 2011 Giant piezoelectricity on Si for hyperactive MEMS *Science* **334** 958–61
[24] Luo L H, Wang H X, Tang Y X, Zhao X Y, Feng Z Y, Lin D and Luo H S 2006 Ultrahigh transverse strain and piezoelectric behavior in (1−x)Pb($Mg_{1/3}Nb_{2/3}$)O_3–$x$$PbTiO_3$ crystals *J. Appl. Phys.* **99** 024104
[25] Javed A, Morley N A and Gibbs M R J 2009 Structure, magnetic and magnetostrictive properties of as-deposited Fe-Ga thin films *J. Magn. Magn. Mater.* **321** 2877–82
[26] Morley N A, Javed A and Gibbs M R J 2009 Effect of a forming field on the magnetic and structural properties of thin Fe-Ga films *J. Appl. Phys.* **105** 07A912
[27] França D R and Blouin A 2004 All-optical measurement of in-plane and out-of-plane Young's modulus and Poisson's ratio in silicon wafers by means of vibration modes *Meas. Sci. Technol.* **15** 859–68
[28] Lampenscherf S, Pompe W and Wilkinson D S 2000 Stress development due to capillary condensation in powder compacts: a 2D model study *J. Am. Ceram. Soc.* **83** 1333–40
[29] Fitchorov T, Chen Y, Hu B, Gillette S M, Geiler A, Vittoria C and Harris V G 2011 Tunable fringe magnetic fields induced by converse magnetoelectric coupling in a FeGa/PMN–PT multiferroic heterostructure *J. Appl. Phys.* **110** 123916
[30] Moutis N, Suarez-Sandoval D and Niarchos D 2008 Voltage-induced modification in magnetic coercivity of patterned $Co_{50}Fe_{50}$ thin film on piezoelectric substrate *J. Magn. Magn. Mater.* **320** 1050–5

[31] Zhu G D, Wong K L, Zhao J, Amiri P K, Wang K L, Hockel J, Carman G P, Zhu J and Krivorotov I 2012 The influence of in-plane ferroelectric crystal orientation on electrical modulation of magnetic properties in $Co_{60}Fe_{20}B_{20}/SiO_2/(0\,1\,1)$ xPb$(Mg_{1/3}Nb_{2/3})O_3$-$(1-x)$$PbTiO_3$ heterostructures *J. Appl. Phys.* **112** 033916

[32] Eerenstein W, Wiora M, Prieto J L, Scott J F and Mathur N D 2007 Giant sharp and persistent converse magnetoelectric effects in multiferroic epitaxial heterostructures *Nat. Mater.* **6** 348–51

[33] Jin T L, Hao L, Cao J W, Liu M F, Dang H G, Wang Y, Wu D P, Bai J M and Wei F L 2014 Electric field control of anisotropy and magnetization switching in CoFe and CoNi thin films for magnetoelectric memory devices *Appl. Phys. Express* **7** 043002

[34] Lo C C H, Lee S J, Li L, Kerdus L C and Jiles D C 2002 Modeling stress effects on magnetic hysteresis and barkhausen emission using a hysteretic-stochastic model *IEEE Trans. Magn.* **38** 2418–20

[35] Thiele C, Dörr K, Bilani O, Rödel J and Schultz L 2007 Influence of strain on the magnetization and magnetoelectric effect in $La_{0.7}A_{0.3}MnO_3$/PMN–PT(0 0 1) (A = Sr,Ca) *Phys. Rev.* B **75** 054408

[36] Das S, Herklotz A, Pippel E, Guo E J, Rata D and Dörr K 2015 Strain dependence of antiferromagnetic interface coupling in $La_{0.7}Sr_{0.3}MnO_3/SrRuO_3$ superlattices *Phys. Rev.* B **91** 134405

[37] Vas'ko V A, Rantschler J O and Kief M T 2004 Structure, stress, and magnetic properties of high saturation magnetization films of FeCo *IEEE Trans. Magn.* **40** 2335–7

[38] Duan C G, Jaswal S S and Tsymbal E Y 2006 Predicted magnetoelectric effect in $Fe/BaTiO_3$ multilayers: ferroelectric control of magnetism *Phys. Rev. Lett.* **97** 047201

QUERIES

Page 1
AQ1
Please be aware that the colour figures in this article will only appear in colour in the online version. If you require colour in the printed journal and have not previously arranged it, please contact the Production Editor now.
Page 6
AQ2
Please check the details for any journal references that do not have a link as they may contain some incorrect information.